Epitaxial stabilization of Sr$_3$Ir$_2$O$_7$ thin films (F)

Junyi Yang, Lin Hao, Peyton Nanney, Kyle Noordhoek, Derek Meyers, Lukas Horak, Joshua Sanchez, Jiun-Haw Chu, Christie Nelson, Mark. P. M. Dean (iD), and Jian Liu

COLLECTIONS

(F) This paper was selected as Featured

View Online   Export Citation   CrossMark

ARTICLES YOU MAY BE INTERESTED IN

Probing the band alignment in rectifying SrIrO$_3$/Nb:SrTiO$_3$ heterostructures
Applied Physics Letters **114**, 133504 (2019); https://doi.org/10.1063/1.5087956

Large spin-orbit torque observed in epitaxial SrIrO$_3$ thin films
Applied Physics Letters **114**, 232406 (2019); https://doi.org/10.1063/1.5097699

Artifact-free optical spin–orbit torque magnetometry
Applied Physics Letters **114**, 182402 (2019); https://doi.org/10.1063/1.5087743

Epitaxial stabilization of $Sr_3Ir_2O_7$ thin films

View Online   Export Citation   CrossMark

Junyi Yang,[1,a)] Lin Hao,[1,a)] Peyton Nanney,[1] Kyle Noordhoek,[1] Derek Meyers,[2] Lukas Horak,[3] Joshua Sanchez,[4] Jiun-Haw Chu,[4] Christie Nelson,[5] Mark. P. M. Dean,[2] and Jian Liu[1,a)]

AFFILIATIONS

[1]Department of Physics and Astronomy, University of Tennessee, Knoxville, Tennessee 37996, USA
[2]Department of Condensed Matter Physics and Materials Science, Brookhaven National Laboratory, Upton, New York 11973 USA
[3]Department of Condensed Matter Physics, Charles University, Ke Karlovu 5, 121 16 Prague, Czech Republic
[4]Department of Physics, University of Washington, Seattle, Washington 98105, USA
[5]National Synchrotron Light Source II, Brookhaven National Laboratory, Upton, New York 11973, USA

a)Authors to whom correspondence should be addressed: jyang43@vols.utk.edu; lhao3@utk.edu; and jianliu@utk.edu

ABSTRACT

Ruddlesden-Popper type $Sr_{n+1}Ir_nO_{3n+1}$ compounds are a major focus of condensed matter physics, where the subtle balance between electron-electron correlation, spin–orbit interaction, and crystal field effect brings a host of emergent phenomena. While it is understandable that a canted antiferromagnetic insulating state with an easy-plane anisotropy is developed in Sr_2IrO_4 as the two-dimensional limit of the series, it is intriguing that bilayer $Sr_3Ir_2O_7$, with slightly higher effective dimensionality, stabilizes c-axis collinear antiferromagnetism. This also renders $Sr_3Ir_2O_7$ a unique playground to study exotic physics near a critical spin transition point. However, the epitaxial growth of $Sr_3Ir_2O_7$ is still a challenging task because of the narrow growth window. In our research, we have studied the thermodynamic process during the synthesis of $Sr_3Ir_2O_7$ thin films. We expanded the synthesis window by mapping out the relationship between the thin film crystal structure and the gas pressure. Our work thus provides a more accessible avenue to stabilize metastable materials.

Published under license by AIP Publishing. https://doi.org/10.1063/1.5092614

Layered compounds of Ruddlesden-Popper (RP) oxides $A_{n+1}B_nO_{3n+1}$ are a fertile playground to study and engineer the interplay of electronic and magnetic properties with crystal lattice dimensionality.[1–5] The crystal structure of the RP series can be viewed as n consecutive ABO_3 perovskite layers sandwiched by rock-salt AO layers along the c-axis. When n varies from 1 to infinity, the lattice undergoes an evolution from the quasi-two-dimensional (2D) limit to the three-dimensional (3D) limit, leading to a dimensional crossover of electronic and magnetic interactions.[6–12] For example, the 2D limit of the iridate RP family, Sr_2IrO_4 [Fig. 1(a)], represents a spin–orbit coupled Mott insulator.[13,14] The subtle balance between spin–orbit coupling, onsite Coulomb repulsion, and crystal field effect leads to a pseudospin $J_{eff} = 1/2$ moment on each Ir site that orders antiferromagnetically within the 2D perovskite layer with an easy ab-plane anisotropy and spin canting.[14–17] The magnetic structure is extremely sensitive to the dimensionality, as a slight increase in n to 2 stabilizes the c-axis collinear antiferromagnetic (AFM) insulating state in $Sr_3Ir_2O_7$ [Fig. 1(a)], rendering a dimensionality-controlled spin flop transition.[18,19] When further moving toward the 3D limit, the insulating ground state melts into a topological semimetallic state in paramagnetic $SrIrO_3$ [Fig. 1(a)].[10–12,20–22]

To study and control the emergent phenomena within the dimensional crossover, epitaxial growth of the RP series is a particularly appealing route due to additional tunability of the lattice structure, such as imposing epitaxial strain.[23–31] However, while epitaxial thin films of Sr_2IrO_4 and $SrIrO_3$ can be readily obtained and have been characterized by many techniques,[23–27,30,32–34] epitaxial growth of $Sr_3Ir_2O_7$ is much more challenging. It was reported that by using a single $SrIrO_3$ target, the $Sr_3Ir_2O_7$ phase can be obtained through careful control of the oxygen pressure and the temperature within a small region of the parameter space.[35] The low thermodynamic stability and the narrow growth window of the $Sr_3Ir_2O_7$ phase were later confirmed by using a target of the $Sr_3Ir_2O_7$ phase.[36] On the other hand, the magnetic ordering of the $Sr_3Ir_2O_7$ thin films remains unclear.

In this work, we performed a systematic investigation of the thermodynamic stability of the iridate RP series in relation to the growth atmosphere. By using a target of the Sr_2IrO_4 phase, we were able to obtain high-quality thin films of single phase Sr_2IrO_4, $Sr_3Ir_2O_7$, and $SrIrO_3$ by varying the pure oxygen pressure. Magnetometry and magnetic resonant scattering experiments demonstrate that the obtained $Sr_3Ir_2O_7$ film retains the same antiferromagnetic ground state as the single crystal counterpart. The obtained growth window of the

FIG. 1. (a) Schematic crystal structures of Sr_2IrO_4, $Sr_3Ir_2O_7$, and $SrIrO_3$. (b) X-Ray diffraction $\theta - 2\theta$ plots of representative samples with distinct RP phases. An offset is added to each plot for better presentation.

$Sr_3Ir_2O_7$ phase in a pure oxygen atmosphere is narrow and similar to the previous reports on $SrIrO_3$ and $Sr_3Ir_2O_7$ targets. By introducing argon into the growth atmosphere, we found a significant expansion of the growth window as a function of oxygen partial pressure.

$Sr_{n+1}Ir_nO_{3n+1}$ thin films with thickness around $100\,nm$ were deposited on $SrTiO_3$ (001) (STO, $a_{pc} = 3.905\,Å$) single crystal substrates by using a pulsed laser deposition system (KrF excimer laser). During deposition, the laser fluence was kept at $3\,J/cm^2$. The growth temperature was chosen to be $850\,°C$ in order to maximize the synthesis window of the $Sr_3Ir_2O_7$ phase based on a previous report.[35] Two independent experiments were performed in pure oxygen and argon-mixed oxygen atmospheres by varying the growth pressure from $1\,mTorr$ to $120\,mTorr$. The crystal structure and the crystallinity of the thin films were investigated by X-ray diffraction (XRD) measurements on a Panalytical X'Pert MRD diffractometer using Cu Kα radiation (1.5406 Å). Magnetic property measurements were carried out on a Vibrating Sample Magnetometer (Quantum Design). The dc resistivity was measured by using the standard four-point probe on a Physical Property Measurement System (Quantum Design). Synchrotron X-ray resonant magnetic scattering experiments were performed on NSLS-II beamline 4-ID at Brookhaven National Laboratory.

Figure 1(b) shows representative XRD patterns of thin films grown in a pure oxygen atmosphere but with different pressures. At the lowest pressure value used in this study ($1\,mTorr$), only a

set of $(0\,0\,L)$ Bragg reflections that corresponds to the Sr_2IrO_4 phase can be seen. This observation indicates the epitaxial growth of Sr_2IrO_4 on the $SrTiO_3$ substrate along the [001] direction without observable impurity phases. The single Sr_2IrO_4 phase is also observed at $10\,mTorr$ and $20\,mTorr$, which is consistent with previous reports.[35] At $80\,mTorr$ and $100\,mTorr$, a different phase appears with all the film peaks that can be indexed as the $(0\,0\,L)$ Bragg reflections of the $Sr_3Ir_2O_7$ phase. A further increase of the growth pressure to $120\,mTorr$ suppresses the $Sr_3Ir_2O_7$ phase and leaves only a set of film peaks near the substrate $(0\,0\,L)$ peaks, characteristic of a single $SrIrO_3$ perovskite phase.[37,38] The Bragg reflections of the $Sr_3Ir_2O_7$ phase are broader than those of the Sr_2IrO_4 and $SrIrO_3$ phases, indicating the possible presence of stacking faults in the $Sr_3Ir_2O_7$ phase and consistent with previous reports.[35] These results indicate that not only the $n = 1$ and $n = \infty$ structures of the RP series can be epitaxially grown by using a Sr_2IrO_4 target, the $n = 2$ structure can also be stabilized by carefully varying the atmosphere pressure.

To further elucidate on this point, we performed detailed physical property measurements. Figure 2(a) displays the temperature dependent resistivity of the $Sr_3Ir_2O_7$ and Sr_2IrO_4 films. The monotonic increase in resistivity with decreasing temperature reveals the insulating state of both thin films. The $Sr_3Ir_2O_7$ film is evidently less insulating than the Sr_2IrO_4 film considering the smaller room-temperature resistivity and the relatively weaker insulating temperature dependence, consistent with the reports on the bulk counterparts.[39–41] The observation indicates that the dimensionality evolution of the electronic ground state of the iridate RP phases was preserved in thin films. A resistivity anomaly was also observed for the $Sr_3Ir_2O_7$ thin film at $T \sim 250\,K$. From the relationship between $d(\ln\rho)/d(1/T)$ and T [inset of Fig. 2(a)], a λ-like cusp can be clearly seen, suggesting a

FIG. 2. (a) Temperature dependent resistivity of Sr_2IrO_4 (circle) and $Sr_3Ir_2O_7$ (triangle) thin films. The resistivity kink of the $Sr_3Ir_2O_7$ thin film is indicated with a blue arrow. The inset shows the temperature dependence of $d(\ln\rho)/d(1/T)$ of the $Sr_3Ir_2O_7$ thin film. A clear λ-like cusp can be observed. (b) Temperature dependence of the magnetic moment per Ir of Sr_2IrO_4 and $Sr_3Ir_2O_7$ thin films measured under a $0.5\,T$ in-plane magnetic field. (c) L-scan around the $(-0.5\,0.5\,24)$ magnetic reflection of the $Sr_3Ir_2O_7$ thin film at $10\,K$ at the Ir L_3-edge. (d) Energy profile of the $(-0.5\,0.5\,24)$ Bragg reflection peak across the Ir L_3-edge at $10\,K$. The error bars denote the statistic error.

significant change in the electronic properties. Figure 2(b) shows the film magnetization as a function of temperature measured under an in-plane magnetic field. The Sr_2IrO_4 film displays a weak but nonzero magnetization when temperature cools below 210 K. Note that the net magnetization of Sr_2IrO_4 is due to spin-canting of the antiferromagnetically coupled $J_{eff} = 1/2$ moments.[13–16] The magnetic measurement thus implies an antiferromagnetic transition of the Sr_2IrO_4 film with the Neel transition temperature $T_N = 210$ K. In contrast, there is no comparable jump in magnetization in the $Sr_3Ir_2O_7$ film even down to the base temperature of 10 K.

While the absence of net magnetization along with the resistivity kink observed in the thin film is compatible with a collinear antiferromagnetic configuration as reported for $Sr_3Ir_2O_7$ single crystals,[18,19,30] direct verification of the antiferromagnetic ordering is usually highly challenging for thin film samples. To this end, we exploited x-ray magnetic resonant scattering, which has been proven to be a powerful probe of the magnetic structure of iridates due to element selectivity and resonant enhancement.[13] By tuning the x-ray photon energy to the Ir L_3-edge, we performed magnetic resonant scattering measurements on the $Sr_3Ir_2O_7$ film at 10 K. The $(-0.5 \ 0.5 \ 24)$ AFM Bragg peak was clearly identified by the L-scan, as shown in Fig. 2(c), directly demonstrating that the Ir moments are antiferromagnetically ordered within each IrO_2 plane. Figure 2(d) shows the energy profile at the representative magnetic reflection across the Ir L_3-edge. A clear resonant effect can be seen, at energies slightly lower than the Ir L_3 white line similar to other iridium compounds,[13,42,43] confirming the dominant role of Ir ions in developing the long-range magnetic ordering. This observation agrees well with the G-type AFM structure as reported in a $Sr_3Ir_2O_7$ single crystal.[18,19,44,45] Along with the structural analysis, we conclude that the as-obtained film under intermediate pressure indeed has a single $Sr_3Ir_2O_7$ phase.

The growth evolution of the RP phases as a function of oxygen atmosphere pressure is summarized in the left panel of Fig. 3(a). As the oxygen pressure increases from 1 mTorr to 100 mTorr, the obtained thin film evolves from a single Sr_2IrO_4 phase to a single $Sr_3Ir_2O_7$ phase. Between these two single phases, there is an intermediate region where a mixed phase is observed. The growth window of the pure $Sr_3Ir_2O_7$ phase is relatively narrow and spans a range of ~20 mTorr only. To enlarge the growth window, we systematically tuned the oxygen partial pressure while fixing the total atmosphere pressure to 100 mTorr by introducing different amounts of argon into the chamber. Five oxygen partial pressures 80 mTorr, 50 mTorr, 20 mTorr, 10 mTorr, and 0 mTorr were selected for this study. Starting from the high oxygen partial pressure $P_O = 80$ mTorr ($P_{Ar} = 20$ mTorr), the obtained thin film displays a single $Sr_3Ir_2O_7$ phase [Fig. 3(b)], which is the same as that in a pure oxygen atmosphere with $P_o = 80$ mTorr. With the decrease of P_O down to 50 mTorr ($P_{Ar} = 50$ mTorr), interestingly, the obtained thin film still shows only the set of Bragg reflections that characterizes a $Sr_3Ir_2O_7$ single phase. This is in sharp contrast to the mixed phase film synthesized under a pure oxygen atmosphere of the same $P_o = 50$ mTorr [Fig. 3(c)]. As P_O decreases further down to 20 mTorr ($P_{Ar} = 80$ mTorr) and 10 mTorr ($P_{Ar} = 90$ mTorr), the $Sr_3Ir_2O_7$ phase remains robust although the Bragg reflections are broadened [Figs. 3(c) and 3(d)]. In other words, the thermal stability of the $Sr_3Ir_2O_7$ phase has been significantly enhanced by introducing argon. On the other hand, in a pure argon atmosphere, i.e., $P_o = 0$ mTorr, none of the above RP phases can be
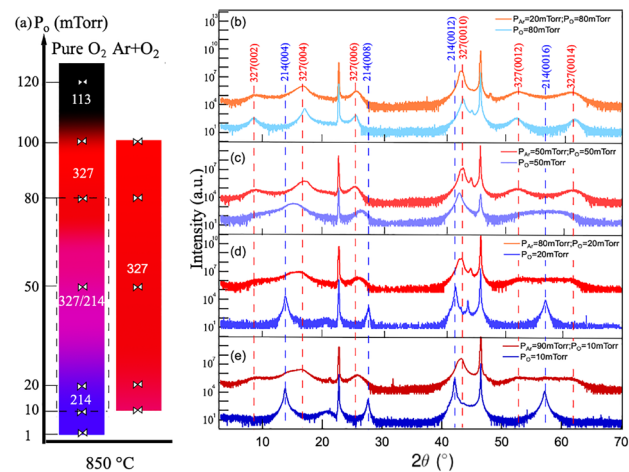

FIG. 3. (a) Growth phase diagram of $Sr_{n+1}Ir_nO_{3n+1}$ thin films. The left panel summaries the results obtained under a pure oxygen atmosphere and the dashed rectangle highlights the oxygen partial pressure range of interest, from 10 to 80 mTorr. The right panel shows the results obtained under an argon-mixed oxygen atmosphere. The black, red, and blue regions denote, respectively, where a single phase of $SrIrO_3$, $Sr_3Ir_2O_7$, and Sr_2IrO_4 is observed. The Sr_2IrO_4 and $Sr_3Ir_2O_7$ phases-mixed region is drawn as pink. Batwing markers label synthesized thin films. X-Ray diffraction $\theta - 2\theta$ plots of thin film samples synthesized under $P_O = 80$ mTorr (b), 50 mTorr (c), 20 mTorr (d), and 10 mTorr (e) in pure oxygen and argon-mixed oxygen atmospheres. Plots of samples grown in a mixed atmosphere are vertically shifted for clarity.

synthesized, highlighting the critical role of oxygen in stabilizing a $Sr_{n+1}Ir_nO_{3n+1}$ phase. The growth evolution as a function of P_O within a mixed atmosphere is sketched in the right panel of Fig. 3(a). As compared to that obtained in a pure oxygen atmosphere, it is clear that the growth window of the $Sr_3Ir_2O_7$ phase has been greatly expanded after the introduction of argon.

From the chemical formula $A_{n+1}B_nO_{3n+1}$ of the RP oxides, it can be seen that the B/A cation ratio increases from 0.5 for $n = 1$ to 1 for $n = \infty$. The Sr_2IrO_4 and $Sr_3Ir_2O_7$ phases can be considered as variants of $SrIrO_3$ with different degrees of Ir-deficiency. It is indeed possible for $SrIrO_3$ to decompose into various RP members with the by-product of Ir and O_2, or vice versa. As shown by the previous studies,[35,36] such controllability of the thermodynamic stability of the three RP phases can be achieved during the growth by varying the ambient pressure of pure oxygen, which is also observed in our study. On the other hand, the background pressure of pulsed laser deposition is also known to strongly influence the plasma plume dynamics, including the ratio and the energetics of different ions.[46,47] This effect may also have significant impact on the growth kinetics, such as the sticking coefficients of different ions and species, especially when the pressure is tuned by more than two orders of magnitudes.[46] Such an impact is confirmed by the observed expansion of the growth window of the $Sr_3Ir_2O_7$ phase when the overall pressure is maintained by introducing argon. In other words, when reducing the pressure under a pure oxygen atmosphere, the changes in the thermodynamic phase stability and the plume dynamics both favor the conversion from Ir-rich to Ir-deficient phases. This combination results in a sharp evolution between the two end members, the Sr_2IrO_4 and $SrIrO_3$ phases with a narrow window of the $Sr_3Ir_2O_7$ phase in-between. Indeed, previous studies and ours all found a remarkably similar phase dependence on

the oxygen pressure from the level of 1 mTorr to 100 mTorr regardless of the target stoichiometry. Such a phase evolution is significantly slowed down when the plume dynamics is stabilized by introducing argon to maintain the total pressure, extending the growth window of the $Sr_3Ir_2O_7$ phase.

In conclusion, we systematically investigated the effect of growth atmosphere on the epitaxial growth of $Sr_{n+1}Ir_nO_{3n+1}$ series. The magnetic scattering measurements in combination with structural analysis and physical property measurements enable us to draw the growth phase diagram as a function of oxygen pressure, upon which the narrow growth window of the $Sr_3Ir_2O_7$ phase is highlighted. We demonstrated that this growth window can be greatly expanded by introducing argon into the growth chamber. Although it is well known that pure oxygen is widely used during the oxide synthesis process, the present study affords an efficient route to synthesize a metastable phase during epitaxial growth.

REFERENCES

[1] J. G. Rau, E. K. H. Lee, and H. Y. Kee, Annu. Rev. Condens. Matter Phys. **7**, 195 (2016).

[2] G. Cao and P. Schlottmann, Rep. Prog. Phys. **81**, 042502 (2018).

[3] S. J. Moon, H. Jin, K. W. Kim, W. S. Choi, Y. S. Lee, J. Yu, G. Cao, A. Sumi, H. Funakubo, C. Bernhard, and T. W. Noh, Phys. Rev. Lett. **101**, 226402 (2008).

[4] Q. Wang, Y. Cao, J. A. Waugh, S. R. Park, T. F. Qi, O. B. Korneta, G. Cao, and D. S. Dessau, Phys. Rev. B **87**, 245109 (2013).

[5] I. Pallecchi, M. T. Buscaglia, V. Buscaglia, E. Gilioli, G. Lamura, F. Telesio, M. R. Cimberle, and D. Marre, J. Phys.: Condens. Matter **28**, 065601 (2016).

[6] G. Cao, J. Bolivar, S. McCall, J. E. Crow, and R. P. Guertin, Phys. Rev. B **57**, R11039(R) (1998).

[7] S. Chikara, O. Korneta, W. P. Crummett, L. E. DeLong, P. Schlottmann, and G. Cao, Phys. Rev. B **80**, 140407(R) (2009).

[8] S. Fujiyama, H. Ohsumi, T. Komesu, J. Matsuno, B. J. Kim, M. Takata, T. Arima, and H. Takagi, Phys. Rev. Lett. **108**, 247212 (2012).

[9] S. J. Moon, H. Jin, W. S. Choi, J. S. Lee, S. S. A. Seo, J. Yu, G. Cao, T. W. Noh, and Y. S. Lee, Phys. Rev. B **80**, 195110 (2009).

[10] G. Cao, V. Durairaj, S. Chikara, L. E. DeLong, S. Parkin, and P. Schlottmann, Phys. Rev. B **76**, 100402(R) (2007).

[11] Y. F. Nie, P. D. C. King, C. H. Kim, M. Uchida, H. I. Wei, B. D. Faeth, J. P. Ruf, L. Xie, X. Pan, C. J. Fennie, D. G. Schlom, and K. M. Shen, Phys. Rev. Lett. **114**, 016401 (2015).

[12] J. Fujioka, T. Okawa, A. Yamamoto, and Y. Tokura, Phys. Rev. B **95**, 121102(R) (2017).

[13] B. J. Kim, H. Ohsumi, T. Komesu, S. Sakai, T. Morita, H. Takagi, and T. Arima, Science **323**, 1329 (2009).

[14] B. J. Kim, H. Jin, S. J. Moon, J.-Y. Kim, B. G. Park, C. S. Leem, J. Yu, T. W. Noh, C. Kim, S. J. Oh, J. H. Park, V. Durairaj, G. Cao, and E. Rotenberg, Phys. Rev. Lett. **101**, 076402 (2008).

[15] G. Jackeli and G. Khaliullin, Phys. Rev. Lett. **102**, 017205 (2009).

[16] F. Wang and T. Senthil, Phys. Rev. Lett. **106**, 136402 (2011).

[17] H. Jin, H. Jeong, T. Ozaki, and J. Yu, Phys. Rev. B **80**, 075112 (2009).

[18] J. W. Kim, Y. Choi, J. Kim, J. F. Mitchell, G. Jackeli, M. Daghofer, J. van den Brink, G. Khaliullin, and B. J. Kim, Phys. Rev. Lett. **109**, 037204 (2012).

[19] S. Boseggia, R. Springell, H. C. Walker, A. T. Boothroyd, D. Prabhakaran, D. Wemeille, S. P. Collins, and D. F. McMorrow, J. Phys.: Condens. Matter **24**, 312202 (2012).

[20] J. M. Carter, V. V. Shankar, M. Ahsan Zeb, and H. Y. Kee, Phys. Rev. B **85**, 115105 (2012).

[21] Z. T. Liu, M. Y. Li, Q. F. Li, J. S. Liu, W. Li, H. F. Yang, Q. Yao, C. C. Fan, X. G. Wan, Z. Wang, and D. W. Shen, Sci. Rep. **6**, 30309 (2016).

[22] M. Ahsan Zeb and H.-Y. Kee, Phys. Rev. B **86**, 085149 (2012).

[23] A. Biswas, K.-S. Kim, and Y. H. Jeong, J. Appl. Phys. **116**, 213704 (2014).

[24] K. R. Kleindienst, K. Wolff, J. Schubert, R. Schneider, and D. Fuchs, Phys. Rev. B **98**, 115113 (2018).

[25] J. Liu, D. Kriegner, L. Horak, D. Puggioni, C. Rayan Serrao, R. Chen, D. Yi, C. Frontera, V. Holy, A. Vishwanath, J. M. Rondinelli, X. Marti, and R. Ramesh, Phys. Rev. B **93**, 085118 (2016).

[26] C. Rayan Serrao, J. Liu, J. T. Heron, G. Singh-Bhalla, A. Yadav, S. J. Suresha, R. J. Paull, D. Yi, J.-H. Chu, M. Trassin, A. Vishwanath, E. Arenholz, C. Frontera, J. Železný, T. Jungwirth, X. Marti, and R. Ramesh, Phys. Rev. B **87**, 085121 (2013).

[27] J. Nichols, O. B. Korneta, J. Terzic, L. E. De Long, G. Cao, J. W. Brill, and S. S. A. Seo, Appl. Phys. Lett. **103**, 131910 (2013).

[28] B. Kim, P. Liu, and C. Franchini, Phys. Rev. B **95**, 024406 (2017).

[29] A. Lupascu, J. P. Clancy, H. Gretarsson, Z. Nie, J. Nichols, J. Terzic, G. Cao, S. S. A. Seo, Z. Islam, M. H. Upton, J. Kim, D. Casa, T. Gog, A. H. Said, V. M. Katukuri, H. Stoll, L. Hozoi, J. van den Brink, and Y.-J. Kim, Phys. Rev. Lett. **112**, 147201 (2014).

[30] J. Nichols, J. Terzic, E. G. Bittle, O. B. Korneta, L. E. D. Long, J. W. Brill, G. Cao, and S. S. A. Seo, Appl. Phys. Lett. **102**, 141908 (2013).

[31] L. Miao, H. Xu, and Z. Q. Mao, Phys. Rev. B **89**, 035109 (2014).

[32] C. L. Lu, A. Quindeau, H. Deniz, D. Preziosi, D. Hesse, and M. Alexe, Appl. Phys. Lett. **105**, 082407 (2014).

[33] O. Krupin, G. L. Dakovski, B. J. Kim, J. W. Kim, J. Kim, S. Mishra, Y.-D. Chuang, C. R. Serrao, W. S. Lee, W. F. Schlotter, M. P. Minitti, D. Zhu, D. Fritz, M. Chollet, R. Ramesh, S. L. Molodtsov, and J. J. Turner, J. Phys.: Condens. Matter **28**, 32LT01 (2016).

[34] M. P. M. Dean, Y. Cao, X. Liu, S. Wall, D. Zhu, R. Mankowsky, V. Thampy, X. M. Chen, J. G. Vale, D. Casa, J. Kim, A. H. Said, P. Juhas, R. Alonso-Mori, J. M. Glownia, A. Robert, J. Robinson, M. Sikorski, S. Song, M. Kozina, H. Lemke, I. Patthey, S. Owada, T. Katayama, M. Yabashi, Y. Tanaka, T. Togashi, J. Liu, C. Rayan Serrao, B. J. Kim, L. Huber, C.-L. Chang, D. F. McMorrow, M. Först, and J. P. Hill, Nat. Mater. **15**, 601–605 (2016).

[35] K. Nishio, H. Y. Hwang, and Y. Hikita, APL Mater. **4**, 036102 (2016).

[36] A. Gutiérrez-Llorente, L. Iglesias, B. Rodríguez-González, and F. Rivadulla, APL Mater. **6**, 091101 (2018).

[37] J. M. Longo, J. A. Kafalas, and R. J. Arnott, J. Solid State Chem. **3**, 174 (1971).

[38] L. Horák, D. Kriegner, J. Liu, C. Frontera, X. Martib, and V. Holýa, J. Appl. Cryst. **50**, 385 (2017).

[39] G. Cao, Y. Xin, C. S. Alexander, J. E. Crow, P. Schlottman, M. K. Crawford, R. L. Harlow, and W. Marshall, Phys. Rev. B **66**, 214412 (2002).

[40] S. Fujiyama, K. Ohashi, H. Ohsumi, K. Sugimoto, T. Takayama, T. Komesu, M. Takata, T. Arima, and H. Takagi, Phys. Rev. B **86**, 174414 (2012).

[41] N. S. Kini, A. M. Strydom, H. S. Jeevan, C. Geibel, and S. Ramakrishnan, J. Phys.: Condens. Matter **18**, 8205 (2006).

[42] S. Boseggia, R. Springell, H. C. Walker, H. M. Rønnow, C. Rüegg, H. Okabe, M. Isobe, R. S. Perry, S. P. Collins, and D. F. McMorrow, Phys. Rev. Lett. **110**, 117207 (2013).

[43] H. Sagayama, D. Uematsu, T. Arima, K. Sugimoto, J. J. Ishikawa, E. O'Farrell, and S. Nakatsuji, Phys. Rev. B **87**, 100403(R) (2013).

[44]S. Boseggia, R. Springell, H. C. Walker, A. T. Boothroyd, D. Prabhakaran, D. Wermeille, L. Bouchenoire, S. P. Collins, and D. F. McMorrow, Phys. Rev. B **85**, 184432 (2012).

[45]C. Dhital, S. Khadka, Z. Yamani, C. de la Cruz, T. C. Hogan, S. M. Disseler, M. Pokharel, K. C. Lukas, W. Tian, C. P. Opeil, Z. Wang, and S. Wilson, Phys. Rev. B **86**, 100401(R) (2012).

[46]R. Eason, *Pulsed Laser Deposition of Thin Films: Applications-Led Growth of Function Materials* (John Wiley & Sons, Inc, HoboKen, New Jersey, 2007).

[47]J. C. Miller and R. F. Haglund, Jr., *Experimental Methods in the Physical Sciences, Volume 30, Laser Ablation and Deposition* (Academic Press, San Diego, 1998).